Zener Tunneling and Photocurrent Generation in Suspended Quasi-Metallic Carbon Nanotube *pn*-Devices: Supplementary Information

Moh. R. Amer[1], Shun-Wen Chang[3], Rohan Dhall[1], Jing Qiu[2], and Stephen B. Cronin[1,2,3]*

Departments of and Electrical Engineering[1], Material Science[2], Physics and Astronomy[3], University of Southern California, Los Angeles, CA, 90089

Table of Contents:

1- Additional Information on the Device Structure:

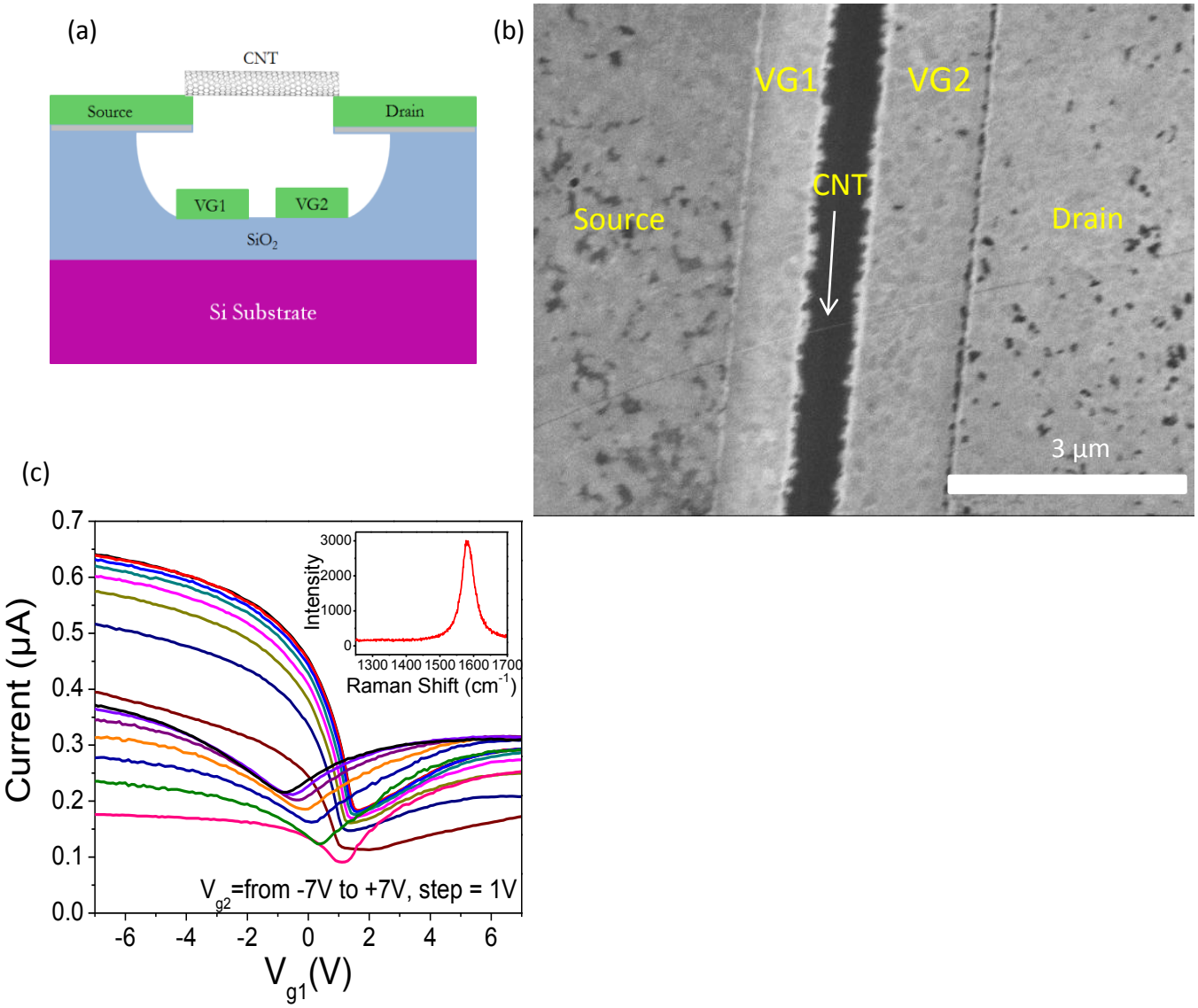

Figure S1. Quasi-Metallic nanotube device structure. (a) Schematic diagram showing the final device structure. (b) SEM image of the suspended nanotube device. (c) V_{g1} sweeps at different V_{g2} sweeps. The charge neutrality points shift with different electrostatic doping. This effect will cause the insulating region position to slightly vary along the length of the nanotube. The inset shows the *G*-band Raman active mode exhibiting Kohn anomaly, indicative of a metallic nanotube.

2- Energy band diagram of each region in the measured rectifying I-V_{bias}:

The band diagram of the rectifying I-V_{bias} when the quasi-metallic nanotube is doped in a *pn* configuration is shown in figure S2 for each different highlighted regime.

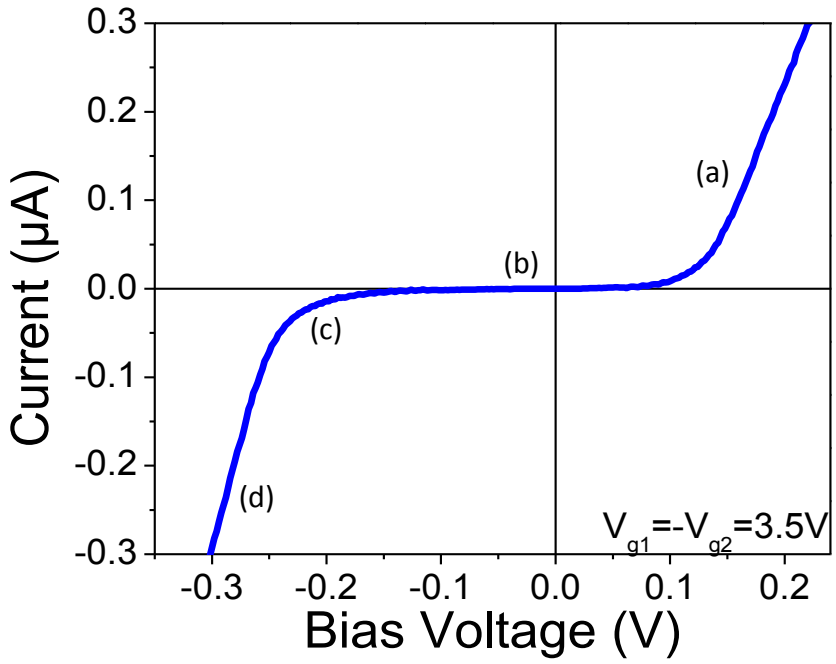

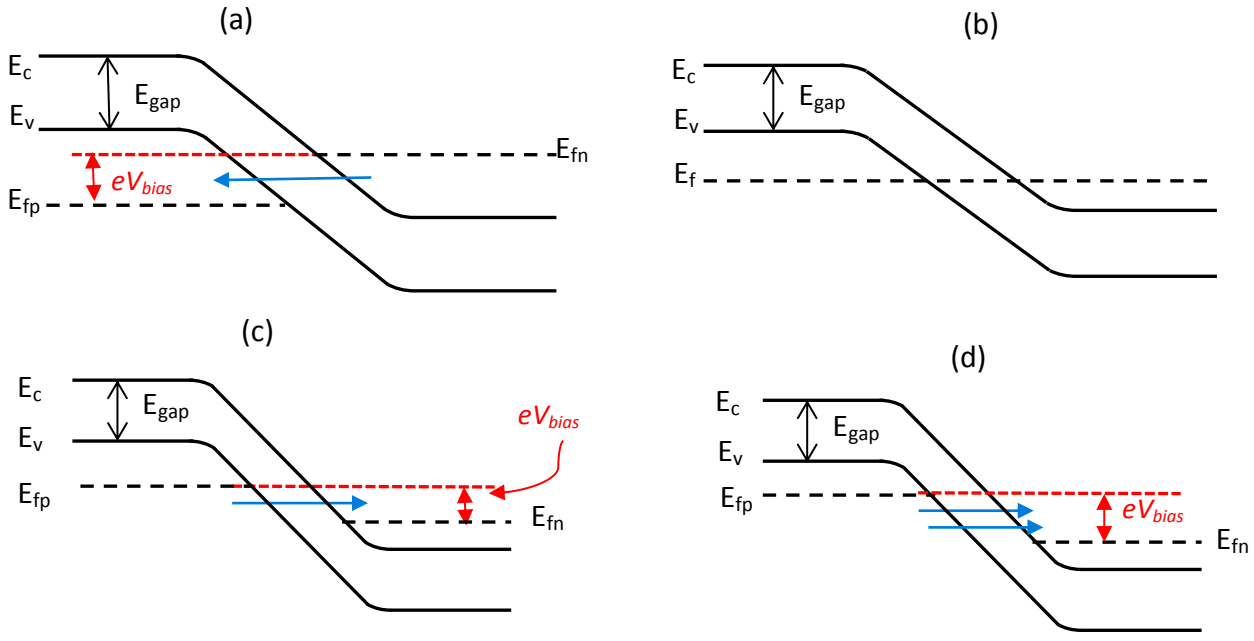

Figure S2. Energy band diagram of forward and reverse biases for a *pn* gated metallic nanotube. The band diagram of each highlighted region on the IV_{bias} curve drawn for illustrative purposes for the case of (a) positive V_{bias}, (b) V_{bias}, = 0 V, (c) negative V_{bias}, and (d) high negative V_{bias}.

3- Additional Zener model fits for different electrostatic doping conditions:

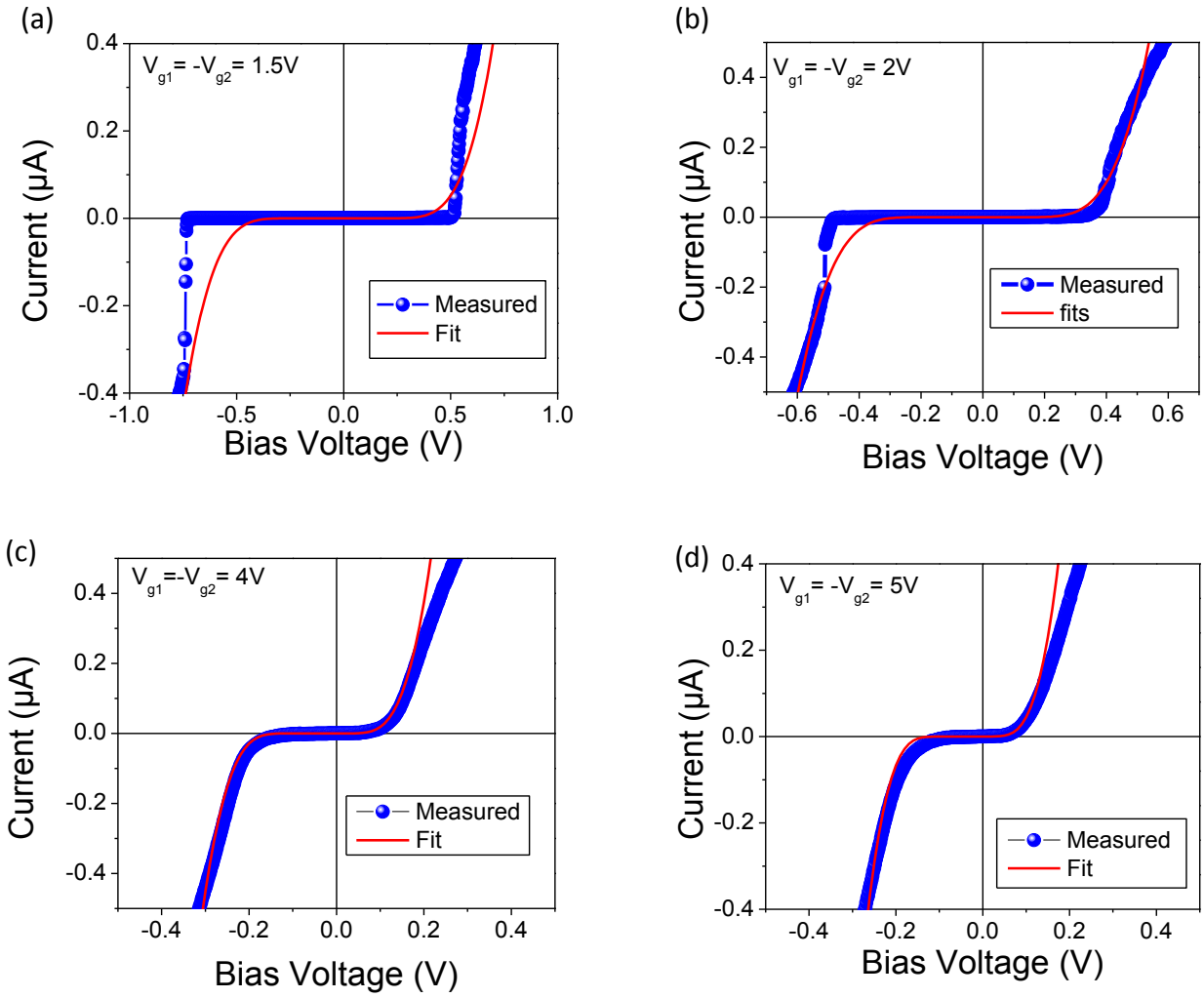

Figure S3. Zener model and measured rectifying *I-V*$_{bias}$. Zener model fits for different electrostatic doping conditions (V_{g1}=-V_{g2}). (a) 1.5*V*, (b) 2*V*, (c) 4*V*, and (d)5*V*. The fitting parameters used to generate these fits are plotted in figure 3c. As discussed in the main paper, the fits agree well for high electrostatic doping conditions as compared to lower doping conditions.

4- Photocurrent Power Dependence and Photocurrent Spectra of Additional Quasi-Metallic Samples with Different Mini-Band Gaps:

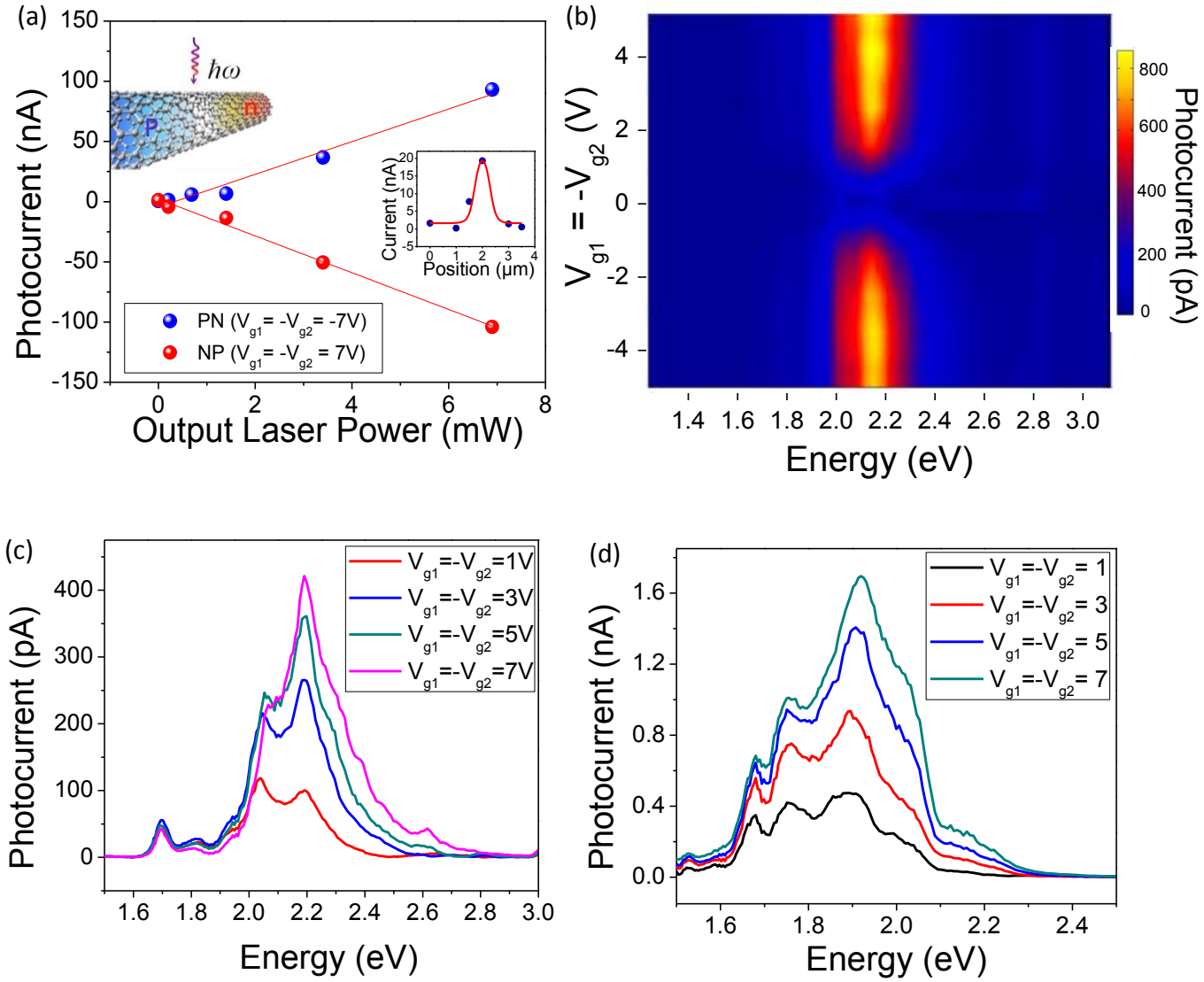

Figure S4. Photocurrent power dependence and photocurrent spectra at room temperature. (a) *pn* and *np* power dependence of the nanotube showing a linear dependence which rolls out the effect of the thermally generated current. A 633nm laser is used with the laser spot centered in the middle of the nanotube as illustrated in the graphical inset. The laser output power was measured using a silicon photodiode while neutral density filters are used to vary the output power. The inset figure shows the spatial photocurrent scan along the length of a 4μm long nanotube when biased in a *pn* configuration. The photocurrent peaks in the middle section of the nanotube indicating of a charge separation region. (b) Photocurrent spectra map of the sample in figure 1c with additional doping conditions showing a peak occurring at 2.14*eV* (c,d) Photocurrent spectra of 2 different quasi-metallic samples taken at different gating conditions. The spectra show the evolution of prominent peaks which are attributed to E_{ii} in accordance with the photocurrent peak observed in figure 1c and S1b.

5- Switching Between Ohmic Behavior and Rectifying Behavior, and Tunable Rectifying Behavior of Additional Quasi-Metallic Samples with narrower mini-band gaps:

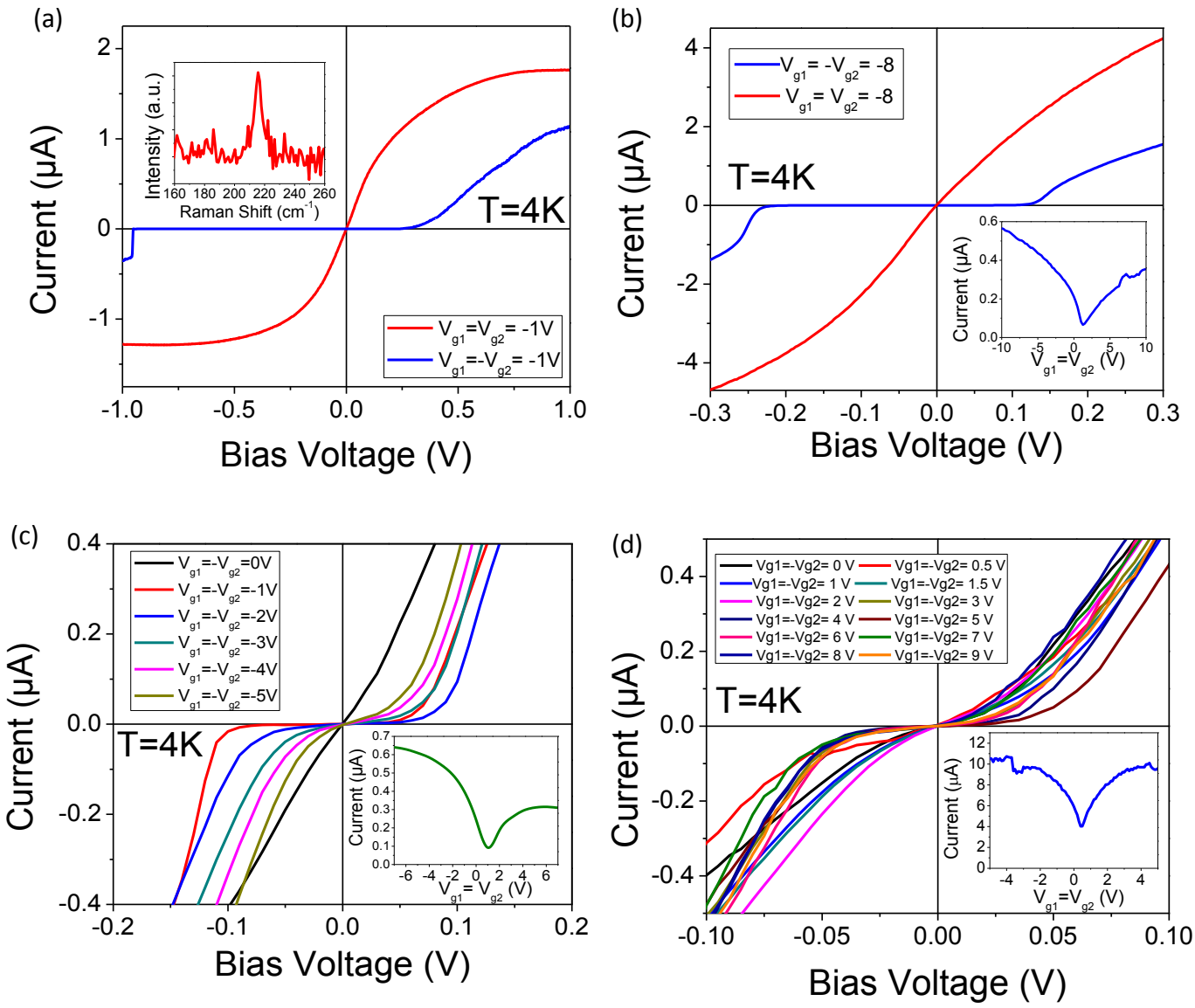

Figure S5. Current-Voltage characteristics at 4K of additional samples. (a) I-V_{bias} at 4K of the sample in figure 2 showing a pronounced rectifying behavior when gated in a *pn* configuration while ohmic behavior is observed when gated in *pp* configuration. The inset shows the Raman RBM peak which gives us the advantage of identifying the chirality of the nanotube along with the photocurrent spectra in figure 1c (b) another sample showing the tunability between ohmic behavior and rectifying behavior at 4K. The inset shows the Current- Gate Voltage characteristics at room temperature. (c,d) tunable rectifying behavior with doping conditions of 2 different quasi-metallic samples at 4K. These samples exhibit narrower band gaps than the samples in figures S3(a,b) (see insets for I-V_{gate} taken at room temperature) further cooperating the strong dependence of Zener tunneling with the quasi-metallic nanotube's mini-band gap.